Available online at www.sciencedirect.com
ScienceDirect
Chemical Physics Letters 452 (2008) 78–83
CHEMICAL PHYSICS LETTERS
www.elsevier.com/locate/cplett

Geometry and excitation energy fluctuations of NMA in aqueous solution with CHARMM, AMBER, OPLS, and GROMOS force fields: Implications for protein ultraviolet spectra simulation

Zhenyu Li [a,1], Haibo Yu [b], Wei Zhuang [a], Shaul Mukamel [a,*]

[a] Department of Chemistry, University of California, Irvine, CA 92697, USA
[b] Department of Chemistry, Theoretical Chemistry Institute, University of Wisconsin, Madison, 1101 University Avenue, Madison, WI 53706, USA

Received 18 November 2007; in final form 10 December 2007
Available online 3 January 2008

Abstract

Molecular dynamics (MD) simulations are performed for *N*-methylacetamide (NMA) in water at 300 K with different force fields. Compared to the three all-atom force fields (CHARMM22, AMBER03, and OPLS-AA), the united-atom force field (GROMOS96) predicts a broader distribution of the peptide OCNH dehedral angle. A map constructed by fitting the $n\pi^*$ and $\pi\pi^*$ transition energies as quadratic functions of the NMA geometric variables is used to simulate the excitation energy fluctuations. GROMOS96 predicts blue shifted $n\pi^*$ and $\pi\pi^*$ energies and stronger fluctuations compared to the other three force fields, which indicates that different force fields may predict different spectral lineshapes for proteins.
© 2007 Elsevier B.V. All rights reserved.

1. Introduction

Ultraviolet (UV) spectra, especially circular dichroism (CD), are important techniques used to probe structure and dynamics of proteins [1,2]. The interpretation of these spectra relies heavily on theoretical simulations. The main challenge in simulating protein spectra is the repeated electronic structure calculation for large systems. *Ab initio* techniques are typically not feasible. A practical way is to construct an exciton model Hamiltonian based on the knowledge of electronic excitations of small chromophores. There are two types of UV chromophores in protein. The first is the aromatic side chains (Phe, Tyr, and Trp), and the second is the peptide units, which form the protein backbone. The latter is closely related to the protein secondary structure. *N*-methylacetamide (NMA) is widely used as a model to mimic the peptide bond. The first two bands of the backbone electronic excitations are $n\pi^*$ ($\sim$220 nm) and $\pi\pi^*$ ($\sim$190 nm) amide bands. Their transition energies give the diagonal elements of the exciton Hamiltonian matrix. The nondiagonal elements, which describe couplings between different peptide units, are typically approximated by electrostatic interactions between transition charge densities. By diagonalizing the Hamiltonian matrix, we can get the transition energies and other properties of excitons. With exciton energies and transition moments, UV spectra can be simulated by response function theory [3].

Protein motions in aqueous environment play an important role in their function [4]. Such fluctuations lead to inhomogeneous broadening of the optical spectra, and a proper description of these fluctuations is important for simulating spectral lineshapes [5]. Different lineshapes may lead to a qualitatively different CD spectrum [6].

* Corresponding author. Fax: +1 949 824 8571.
E-mail address: smukamel@uci.edu (S. Mukamel).
[1] Present address: Hefei National Laboratory for Physical Sciences at Microscale, University of Science and Technology of China, Hefei, Anhui 230026, China.

0009-2614/$ - see front matter © 2007 Elsevier B.V. All rights reserved.
doi:10.1016/j.cplett.2007.12.022

Fluctuations can be simulated by molecular dynamics (MD) techniques [7,8], using a classical force field at finite temperature.

Four force fields are widely used for biomolecular dynamics simulations: CHARMM [9], AMBER [10], OPLS [11], and GROMOS [12]. The general force field expression can be written as [13–15]

$$U = \sum_{\text{bonds}} K_b(b-b_0)^2 + \sum_{\text{angles}} K_\theta(\theta-\theta_0)^2 + \sum_{\text{dehedrals}} K_\chi(1+\cos(n\chi-\delta)) + \sum_{\text{impropers}} K_\phi(\phi-\phi_0)^2 + \sum_{\text{nobonded}} \left[\frac{A_{ij}}{r_{ij}^{12}} - \frac{C_{ij}}{r_{ij}^{6}} + \frac{q_i q_j}{\epsilon r_{ij}}\right], \quad (1)$$

where the last term runs over nonbonded atoms in different molecules or separated by at least three bonds in the same molecules. Electrostatic interactions are included by a Coulomb term, and the van der Waals (vdW) interactions are incorporated by a Lennard-Jones term. Nonbonded interactions separated by exactly three bonds (1–4 interaction) are usually reduced by a scale factor compared to larger separations. The CHARMM force field uses an additional Urey–Bradley term. The OPLS dihedral potential includes higher order (up to 3) Fourier terms. The GROMOS force field uses a fourth power bond stretching potential and a cosine based angle potential to save computational cost.

Comparison of different force fields has been made for conformational dynamics of polypeptides [16,17]. In this Letter, we compare the electronic transition energy fluctuations generated by different force fields, which are necessary for simulating the spectral lineshapes. In Section 2, we describe the computational details. The geometric fluctuations, transition energy map, and energy fluctuations are presented in Section 3. We conclude in Section 4.

2. Computational details

MD simulations were performed for NMA (see Fig. 1) in water with the following force fields: version 22 of CHARMM [9], *ff*03 version of AMBER [18], all-atom version of OPLS [11], and the 45a3 version of GROMOS [12]. Point charges for nonbonded Coulomb interactions are listed in Table 1. SHAKE [19] or LINCS [20] methods were applied to constrain the bond length involving hydrogen atoms. Particle mesh Ewald (PME) method [21] was used for long range electrostatic interaction. All MD simulations started from a 5000 step minimization and 600 ps heat-up from 0 to 300 K. Equilibration (2 ns) was then followed by 2 ns dynamics at the NPT ensemble (1 atmosphere pressure and 300 K) with a 1 fs time step. Structures were recorded every 200 fs for late analysis. For gas phase optimization, we used a 40 Å box.

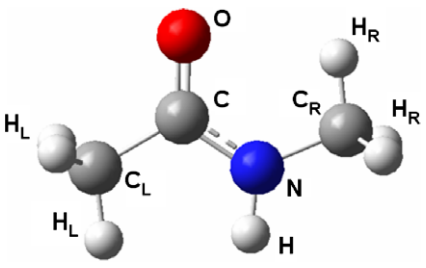

Fig. 1. NMA gas phase geometry optimized at the B3LYP/6-311++G** level of density functional theory.

Table 1
Point charges assigned to each atom in NMA

	CHARMM	AMBER	OPLS-AA	GROMOS
C	0.51	0.5869	0.50	0.38
O	−0.51	−0.5911	−0.50	−0.38
N	−0.47	−0.4192	−0.50	−0.28
H	0.31	0.2823	0.30	0.28
C_L	−0.27	−0.0411	−0.18	0.00
H_L	0.09	0.0173	0.06	N/A
C_R	−0.11	−0.2078	0.02	0.00
H_R	0.09	0.1127	0.06	N/A

CHARMM22: NAMD 2.6 package [22] was used with modified TIP3P water [23]. No general scaling of the 1–4 electrostatic and vdW interactions was used. A switching function was used for nonbonded interactions, with a cutoff radius of 12.0 Å. The equilibrium box has a size of 28.7 Å with 813 water molecules.

AMBER03: AMBER 9 package [24] was used. The 1–4 vdW interaction was scaled by 1/2.0, and 1–4 electrostatic interaction by 1/1.2. The nonbonded interaction was truncated at 12.0 Å. A 29.1 Å equilibrium box with 813 TIP3P water molecules was used.

OPLS-AA: GROMACS 3.3 package [25] was used. The 1–4 nonbonded interactions were scaled by 0.5. Coulomb interactions were truncated at 12.0 Å, and a shift function was used for vdW forces with a cutoff of 14.0 Å. A 30.2 Å equilibrium box with 875 TIP4P water molecules [23] was used.

GROMOS96: The same software package and nonbonded interaction cutoff scheme to the OPLS-AA force field was used. The 1–4 interactions were obtained from a pair list. The equilibrium box has a size of 30.2 Å with 891 SPC water molecules [26].

The excited state properties of NMA were calculated by the time-dependent density functional theory (TDDFT) implemented in the GAUSSIAN 03 package [27]. The hybrid density functional of Perdew, Burke, and Ernzerhof (PBE0) [28] was used. Molecular orbtials were expanded to an atomic basis set 6-311++G**. It is not feasible to include all water molecules in TDDFT. Instead, we mod-

elled the solvation effects by the polarizable continuum model (PCM) [29].

3. Results and discussion

3.1. Geometric fluctuations

The NMA geometry optimized in gas phase at the B3LYP/6-311++G** level is plotted in Fig. 1. The optimized geometric parameters compared in Table 2 shows a good overall agreement with experiment [30]. The main difference is for ∠CNH, where all theoretical predictions are more than 7° larger than experiment. We note that it is difficult to determine the position of H in the electron diffraction experiment [30], and high level quantum chemistry are more reliable in this case.

From the MD trajectories of NMA in aqueous solution, we get the distribution of the geometric variables of NMA (see Fig. 2). In our simulations, the NH bond length is constrained, thus its distribution is very narrow for all force

Table 2
Gas phase geometry

	EXP [30]	B3LYP	CHARMM	AMBER	OPLS-AA	GROMOS
d_{CO}	1.224	1.221	1.223 (1.230)	1.227 (1.229)	1.228 (1.229)	1.231 (1.230)
d_{CN}	1.386	1.367	1.339 (1.345)	1.339 (1.335)	1.338 (1.335)	1.325 (1.330)
d_{NH}	–	1.007	0.993 (0.997)	1.008 (1.010)	1.010 (1.010)	0.992 (1.000)
$d_{C_{LC}}$	1.520	1.519	1.481 (1.490)	1.524 (1.522)	1.528 (1.522)	1.535 (1.530)
d_{NC_R}	1.468	1.454	1.444 (1.430)	1.464 (1.449)	1.456 (1.449)	1.474 (1.470)
∠OCN	121.8	122.9	122.6 (122.5)	122.6 (122.9)	123.0 (122.9)	125.9 (124.0)
∠CNH	110.0	118.4	119.8 (123.0)	117.7 (120.0)	118.4 (119.8)	121.6 (123.0)
$\angle NCC_L$	114.1	115.5	116.4 (116.5)	116.8 (116.6)	117.0 (116.6)	114.3 (115.0)
$\angle CNC_R$	119.6	123.0	121.7 (120.0)	124.0 (121.9)	123.3 (121.9)	119.5 (117.0)
D_{OCNH}	–	180.0	180.0 (180.0)	180.0 (180.0)	180.0 (180.0)	180.0 (180.0)

Distances are in Å, and angles in °. Values in bracket are equilibrium values from the force field bonded interaction parameters.

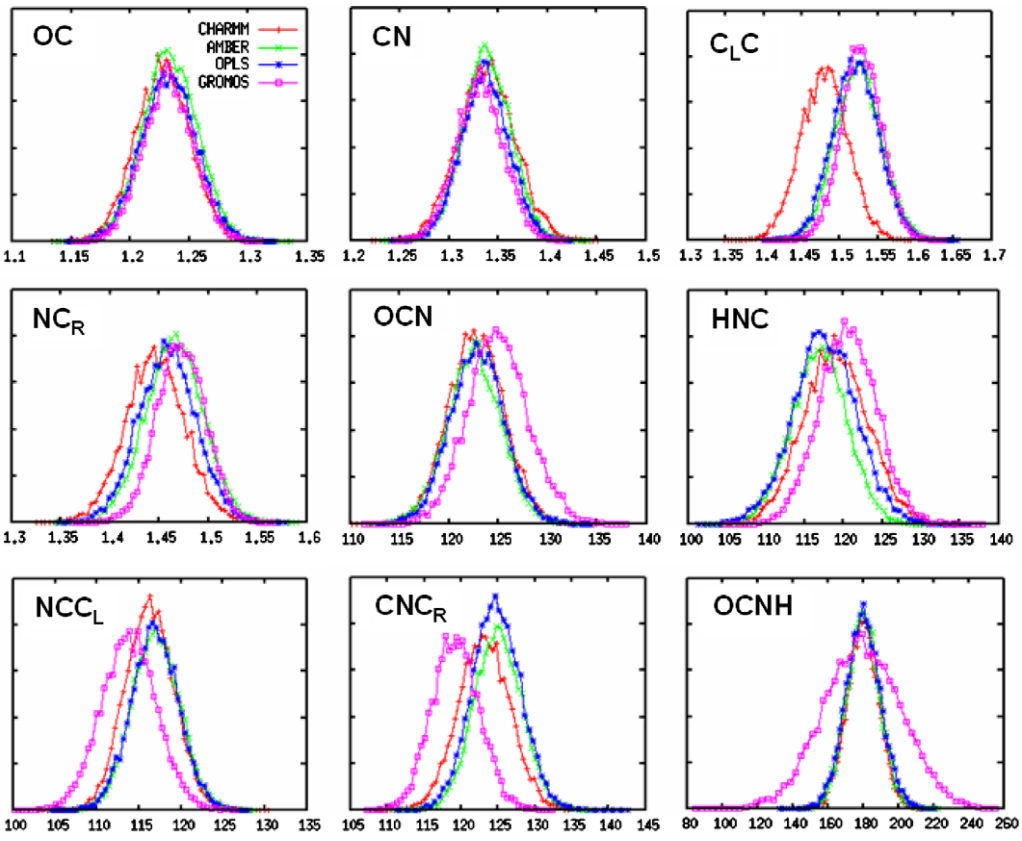

Fig. 2. Distribution of various NMA geometric variables obtained from MD simulations with different force fields.

fields. CHARMM gives shorter C_LC bond length than the other three force fields. The same trend is found in the gas phase geometries. The average angles predicted by GROMOS are shifted compared to the other three force fields, as found in gas phase. Although the averages of the bond and angle distributions for some force fields are shifted, the variances are very similar for all four force fields. However, the distribution of the OCNH dihedral angle is different: all distributions are centered at 180°, but GROMOS yields a much broader distribution. To the best of our knowledge, there is no experimental data on the magnitude of such fluctuations. Infrared spectra on acetamide and acrylamide in gas phase suggested that the resistance to the H out of plane displacement is small [31]. OCNH fluctuations in protein were found to be small [32], possibly because of the constraint of the hydrogen bonds in well defined structural motifs, such as α-helices and β-sheets.

3.2. Transition energy map

Three hundred snapshots of NMA geometries are taken from the CHARMM MD simulation. TDDFT calculations were performed at each geometry to obtain the $n\pi^*$ and $\pi\pi^*$ transition energies. The transition energies were then fitted to a function of the NMA geometric variables. In a previous map, up to cubic terms were used to fit the transition energies, but only four geometric variables were used, and two functions were needed to fit $\pi\pi^*$ energy in different d_{CN} range [33]. To determine a suitable fitting function, we performed several series of TDDFT calculations. In each series, only one geometric variable was varied, and all other geometric variables (bond lengths, angles, and dihedral angles) were held fixed at their optimized geometry values. The calculated transition energies only slightly deviate from linear dependence on all geometric variables, except for the dihedral angle D_{OCNH}. However, as shown in Fig. 3, the cosine of this dihedral angle have a roughly linear relationship with the transition energies. We thus construct the map using the following function:

$$\omega^{\mu} = \omega_0^{\mu} + \sum_{i=1}^{4}\left(\alpha_i^{\mu} d_i + \beta_i^{\mu} d_i^2\right) + \sum_{i=5}^{8}\left(\alpha_i^{\mu}\theta_i + \beta_i^{\mu}\theta_i^2\right) + \alpha_9^{\mu}\cos(\phi) + \beta_9^{\mu}\cos^2(\phi), \quad \mu = n\pi^*, \pi\pi^*, \tag{2}$$

where the four bond lengths d_i are d_{CO}, d_{CN}, d_{C_LC}, and d_{NC_R}, the four angles θ_i are ∠OCN, ∠CNH, $\angle NCC_L$, and $\angle CNC_R$, and the dihedral angle ϕ is D_{OCNH}. d_{NH} is excluded, because in most of MD simulations of proteins, all bonds involving H are fixed. Our test calculations and previous study [34] suggested that the nπ and $\pi\pi^*$ transition energies do not strongly depend on the NH bond length.

The map was obtained by a least-squares fitting. Then, an independent set of other 300 snapshots are used to test the quality of the map by comparing the transition energy calculated directly from TDDFT and from the map. The result is shown in Fig. 4. The Pearson correlation coefficients for $n\pi^*$ and $\pi\pi^*$ are 0.89 and 0.82, respectively.

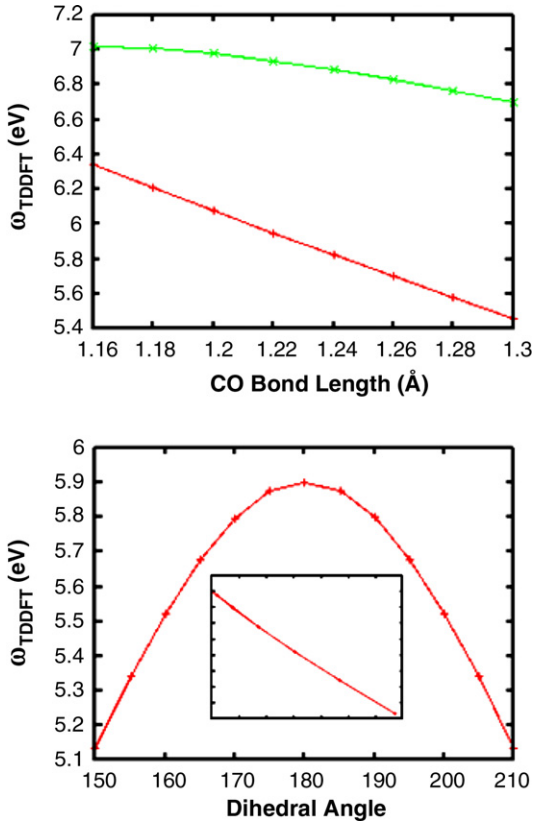

Fig. 3. Upper panel: The TDDFT $n\pi^*$ (red) and $\pi\pi^*$ (green) transition energies ω_{TDDFT} versus the OC bond length. Bottom panel: The TDDFT $n\pi^*$ transition energy ω_{TDDFT} versus the dihedral angle OCNH. Inset: ω_{TDDFT} versus cosine of the dihedral angle. (For interpretation of the references to colour in this figure legend, the reader is referred to the web version of this article.)

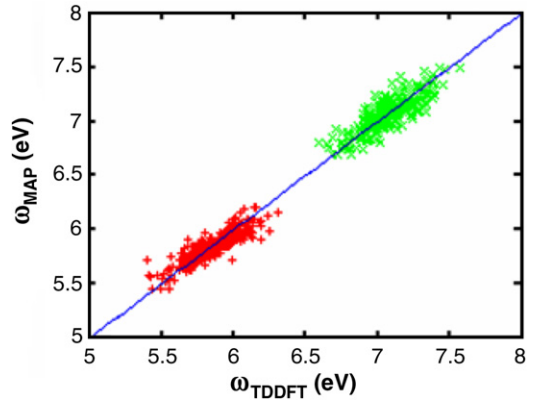

Fig. 4. $n\pi^*$ (red) and $\pi\pi^*$ (green) transition energies of NMA calculated by TDDFT (ω_{TDDFT}) and the map (ω_{MAP}). (For interpretation of the references to colour in this figure legend, the reader is referred to the web version of this article.)

3.3. Transition energy fluctuations

With this map, the nπ and $\pi\pi^*$ transition energies can be calculated at each snapshot in a trajectory. We plot the resulting distributions of the transition energies along the 2 ns trajectories with different force fields in Fig. 5. For

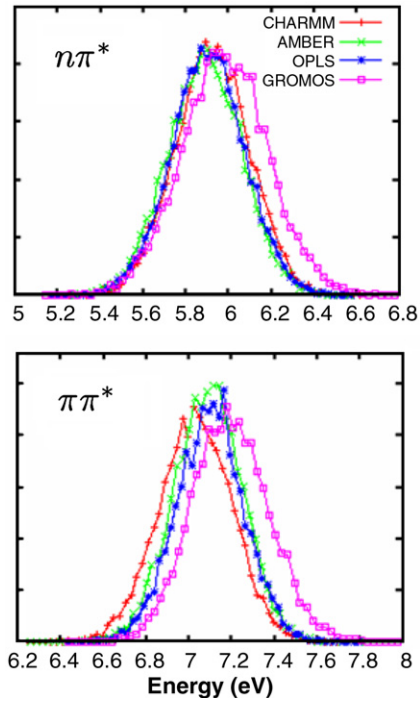

Fig. 5. Distribution of NMA nπ* and ππ* transition energies calculated by the present map using MD trajectories with different force fields.

nπ*, the distributions from the three all-atom force fields are similar. However, GROMOS96 gives a slightly blue shifted and broader distribution. For ππ*, the CHARMM22 distribution is slightly red shifted from AMBER03 and OPLS-AA, and the GROMOS96 distribution is blue shifted and slightly broader than the other three.

Protein UV spectra simulations could then provide a useful test for different force fields. However, the presented transition energy distributions are only one ingredient required for the spectra. In fact, although NMA absorption is dominated by the ππ* transition, its energy distributions by all four force fields are much narrower than the experimental absorption lineshape [35]. To perform a realistic simulation of the spectrum, electrostatic fluctuations from solvent molecules need to be added. Also a map for transition dipoles is required to include their fluctuations caused by geometric and electrostatic fluctuations. Side chains may effect the spectra in the far-UV range too. We are working on developing a protocol for protein UV spectra simulation including fluctuations.

4. Conclusions

The geometry and electronic transition energy fluctuations predicted by four popular biomolecular force fields are compared by a molecular dynamics simulation of NMA in water. The transition energy fluctuations along an MD trajectory can be obtained by constructing a transition energy map. The GROMOS96 force field predicts a broader OCNH dihedral angle distribution and broader nπ* and ππ* transition energy distributions compared to the other three force fields. The fluctuations predicted by different force fields should yield different lineshapes in protein ultraviolet spectra simulations. Techniques sensitive to lineshapes, such as CD, should thus provide a good test for these force fields.

Acknowledgements

This work was supported by the National Institutes of Health Grant GM59230 and the National Science Foundation Grant CHE-0446555.

Appendix A. Supplementary material

Supplementary data associated with this article can be found, in the online version, at doi:10.1016/j.cplett.2007.12.022.

References

[1] K. Nakanishi, N. Berova, R.W. Woody, Circular Dichroism Principles and Applications, VCH, New York, 1994.
[2] G.D. Fasman, Circular Dichroism and the Conformational Analysis of Biomolecules, Plenum, New York, 1996.
[3] S. Mukamel, Principles of Nonlinear Optical Spectroscopy, Oxford University Press, New York, 1995.
[4] D. Kern, E.Z. Eisenmesser, M. Wolf-Watz, Meth. Enzymol. 394 (2005) 507.
[5] A. Glattli, X. Daura, D. Seebach, W.F. van Gunsteren, J. Am. Chem. Soc. 124 (2002) 12972.
[6] Z. Li, D. Abramavicius, W. Zhuang, S. Mukamel, Chem. Phys. 341 (2007) 29.
[7] M. Karplus, J.A. McCammon, Nat. Struct. Biol. 9 (2002) 646.
[8] W.F. van Gunsteren et al., Angew. Chem., Int. Ed. 45 (2006) 4064.
[9] A.D. MacKerell et al., J. Phys. Chem. B 102 (1998) 3586.
[10] J. Wang, P. Cieplak, P. Kollman, J. Comput. Chem. 21 (2000) 1049.
[11] W.L. Jorgensen, D.S. Maxwell, J. Tirado-Rives, J. Am. Chem. Soc. 118 (1996) 11225.
[12] L.D. Schuler, X. Daura, W.F. van Gunsteren, J. Comput. Chem. 22 (2001) 1205.
[13] P.H. Huenenberger, W.F. van Gunsteren, Lect. Notes Chem. 71 (1999) 177.
[14] A.D. MacKerell, J. Comput. Chem. 25 (2004) 1584.
[15] J.W. Ponder, D.A. Case, Adv. Prot. Chem. 66 (2003) 27.
[16] Y. Mu, D.S. Kosov, G. Stock, J. Phys. Chem. B 107 (2003) 5064.
[17] H. Hu, M. Elstner, J. Hermans, Proteins 50 (2003) 451.
[18] Y. Duan et al., J. Comput. Chem. 24 (2003) 1999.
[19] W.F. Vangunsteren, H.J.C. Berendsen, Mol. Phys. 34 (1977) 1311.
[20] B. Hess, H. Bekker, H.J.C. Berendsen, J.G.E.M. Fraaije, J. Comput. Chem. 18 (1997) 1463.
[21] T. Darden, D. York, L. Pedersen, J. Chem. Phys. 98 (1993) 10089.
[22] J.C. Phillips et al., J. Comput. Chem. 26 (2005) 1781.
[23] W.L. Jorgensen, J. Chandrasekhar, J.D. Madura, R.W. Impey, M.L. Klein, J. Chem. Phys. 79 (1983) 926.
[24] D.A. Case et al., J. Comput. Chem. 26 (2005) 1668.
[25] D. van der Spoel, E. Lindahl, B. Hess, G. Groenhof, A.E. Mark, H.J.C. Berendsen, J. Comput. Chem. 26 (2005) 1701.
[26] H.J.C. Berendsen, J.P.M. Postma, W.F. van Gunsteren, J. Hermans, in: B. Pullman (Ed.), Intermolecular Forces, D. Reidel Publishing Company, Dordrecht, 1981, p. 331.
[27] M.J. Frisch et al., Gaussian 03, Revision C.02, Gaussian, Inc., Wallingford, CT, 2004.
[28] J.P. Perdew, M. Ernzerhof, K. Burke, J. Chem. Phys. 105 (1996) 9982.

[29] M. Cossi, V. Barone, B. Mennucci, J. Tomasi, Chem. Phys. Lett. 286 (1998) 253.
[30] M. Kitano, T. Fukuyama, K. Kuchitsu, Bull. Chem. Soc. Jpn. 46 (1973) 384.
[31] R.A. Kydd, A.P.C. Dunham, J. Mol. Struct. 69 (1980) 79.
[32] J.-S. Hu, A. Bax, J. Am. Chem. Soc. 119 (1997) 6360.
[33] N.A. Besley, M.T. Oakley, A.J. Cowan, J.D. Hirst, J. Am. Chem. Soc. 126 (2004) 13502.
[34] J. Sebek, Z. Kejik, P. Bour, J. Phys. Chem. A 110 (2006) 4702.
[35] V. Pajcini, S.A. Asher, J. Am. Chem. Soc. 121 (1999) 10942.